Journal of Biomedical Optics, 2004, 9 (2): 339-346

# Amending of fluorescence sensor signal localization in human skin by matching of the refractive index

**Dmitry Y. Churmakov**
**Igor V. Meglinski**
**Douglas A. Greenhalgh**
Cranfield University
School of Engineering
Cranfield MK43 0AL, United Kingdom

**Abstract.** Fluorescence diagnostic techniques are notable amongst many other optical methods because they offer high sensitivity and noninvasive measurement of tissue properties. However, a combination of multiple scattering and physical heterogeneity of biological tissues hampers interpretation of the fluorescence measurements. Analyses of the spatial distribution of endogenous and exogenous fluorophores excitation within tissues and their contribution to the detected signal localization are essential for many applications. We have developed a novel Monte Carlo technique that gives a graphical perception of how the excitation and fluorescence detected signal are localized in tissues. Our model takes into account the spatial distribution of fluorophores, the variation of concentrations and quantum yield. We demonstrate that matching the refractive indices of the ambient medium and topical skin layer improves spatial localization of the detected fluorescence signal within the tissues.

Keywords: refractive index matching; fluorescence localization; Monte Carlo simulation; sampling volume; skin tissues; tattoo.

## 1 Introduction

The optical properties of skin tissues have been studied for many years and were reviewed by a number of authors over the past decades.[1–5] The growing interest in skin optics is due to the diversity of recently developed noninvasive optical techniques used in modern medicine, both in diagnostics and therapy.[6] The recent progress in physics, biochemistry, optics, and microelectronics has resulted in the successful development of variety of miniature biosensor[7] devices capable of accurate monitoring biochemical parameters, but their application for *in vivo* monitoring remains limited. The reason for this is twofold: (i) difficult integration of artificial sensor elements with living tissue which often results in undesirable immunochemical response and/or fouling of the sensor surface; and (ii) the existing problems in communication between the implanted detector and the sensor.

Recently, a new noninvasive optical/fluorescence technique for express diagnostics and therapeutic monitoring of skin has been proposed as a possible routine clinical diagnostic instrument.[8] The technique is based on scanning a ''tattoo'' pattern transferred onto the skin in a manner similar to children's nonpermanent tattoos. By incorporating ''smart'' polymer nanoparticles in the tattoo formulation it is possible to generate fluorescence signals with specific spectral signatures that are indicative of the state of the tissue. Thus, physiological changes pertaining to the temperature, concentration of metabolites, or presence of drugs can be determined. Since a tattoo can combine several chemical sensors, either by intermixing or by separate patterning onto the skin, multiparameter measurements are possible. This new methodology has considerable potential for clinical application both in hospitals and in surgeries for routine monitoring as well as for more complex therapeutic management of drug administration regimes. Other important potential applications include early warning of excessive exposure to ultraviolet radiation, monitoring of general health, fundamental physiological investigation, measuring sensitivity to cosmetics or household products, detection of allergies etc.

The main advantage of this approach is the opportunity to localize the measurements in a small totally controlled volume that is of particular importance for probing biological tissues. Accordingly, understanding the spatial distribution of fluorescence emission within skin tissue as well as spatial detector depth sensitivity (i.e., sampling volume) is required.

Fluorescence emission is affected by several factors including spatial distribution of the fluorophore and its photophysical parameters (i.e., quantum yield, fluorescence lifetime, etc.)[9] Both excitation and fluorescence radiation that traverse and arise from a volume of tissue are subjected to tissue optics (scattering, absorption, and anisotropy). To elucidate these effects various theoretical models have been developed: electromagnetic theory,[10] Kubelka–Munk approximation,[11] diffusion theory,[12–14] random walk theory,[15] and Monte Carlo (MC) techniques.[16–23] At the same time, autofluorescence properties of human skin *in vivo* were systematically studied and characterized.[24–26] The results demonstrated that the spatial distribution of the skin fluorophores is not uniform, as was assumed in theoretical models,[10–15,24] and has a layered quasiperiodical structure.[19,26]

In this paper, we investigate the distribution of fluorescence emission within skin tissue and the detector depth sen-

Address all correspondence to Dmitry Y. Churmakov. Tel: +44-1234-754767; Fax: +44-1234-750425; E-mail: d.churmakov.2001@cranfield.ac.uk

sitivity, provided that the distribution of skin fluorophores corresponds to the collagen fiber packing. Based on the results of our previous study[27] we pay particular attention to the influence of refractive index matching on changes in the sampling volume. Those results[27] showed that contrast and spatial resolution of the shallow sampling volume produced by the fiber-optic probe can be significantly improved by matching refractive indices at the skin interface. A general MC technique for optical radiation propagation and the fluorescence simulation used to examine the fluorescence excitation and sampling volume in skin tissue are discussed in Secs. 2 and 3, respectively. The results of simulation and discussions are presented in Sec. 4, and conclusions of the study conducted are given in Sec. 5.

## 2 Simulation of Optical Radiation Propagation within Human Skin

The stochastic numerical MC method is widely used to model optical radiation propagation in complex randomly inhomogeneous highly scattering absorbing media like biological tissue.[1,28–31] We employed the MC technique, which combines the statistical weight scheme and optical path simulation.[27,30,31] This simulation approach is based on the modeling of a large number of possible photon packet trajectories from the site of photon injection into the medium (source) to the site where the photons leave the medium (detector). The elements of the simulation of individual photon packet propagation are modeled according to the optical properties of the medium. The initial and final states of the photon packets are determined entirely by the source and detector geometries and their numerical apertures.

Photon path length $l$ can take any positive value with the probability density function[32] $p(l)=\mu_t \exp(-\mu_t l)$, where $\mu_t = \mu_s + \mu_a$, is the extinction coefficient, and $\mu_s$ and $\mu_a$ are the scattering and absorption coefficients, respectively. Assuming independence of the absorption and scattering in the medium, we define a photon packet pathlength at the $i$'th step as

$$l_i = -\frac{\ln(\xi)}{\mu_s}, \tag{1}$$

where $\xi$ is a uniformly distributed random number between 0 and 1. The position of a photon packet is specified in the Cartesian coordinate system. Additionally, the polar $\theta$ and azimuthal $\varphi$ angles are used to describe deviation of the photon packet direction due to scattering at each step of motion in the modeling medium (Fig. 1). Quantitatively, scattering is specified by the anisotropy factor[1] $g$ and the Henyey–Greenstein scattering phase function.[33] A photon packet incident on a medium interface splits into reflected and refracted parts with weight attenuated by[27,30]

$$W = [1 - R_{\text{out}}(\theta_i)][1 - R_{\text{in}}(\theta_i)] W_{\text{in}} \left[ \prod_{p=1}^{M} R(\theta_i) \right], \tag{2}$$

where $W_{\text{in}}$ is the initial weight of the photon packet, $M$ is the number of photon packet reflections/refractions taking place at internal medium interfaces, $R(\theta_i)$ depends on the incident angle $\theta_i$, and denotes the Fresnel reflection/refraction coefficient.[34] When a photon packet enters or leaves the medium, accompanying reflections at the medium interface are described by coefficients $R_{\text{in}}(\theta_i)$ and $R_{\text{out}}(\theta_i)$, respectively.

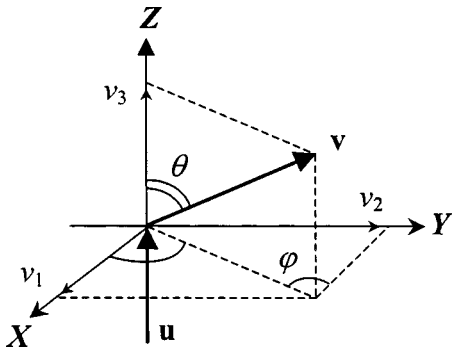



**Fig. 1** Cartesian coordinate system ($XYZ$) employed to specify the position of a photon packet in the modeling medium: **u** and **v** are the directional unit vectors lying along the initial direction of photon packet propagation and a new photon packet direction, respectively. $\theta$ and $\varphi$ are the polar and azimuthal angles of deviation from initial photon direction **u**; $\nu_1$, $\nu_2$, and $\nu_3$ are the directional cosines of the new photon packet direction.

Photon packet tracing is stopped when its statistical weight is less than $10^{-4}$, or when a photon packet has undergone scattering more than $10^4$ times. With regard to these options we assume that the weight is too small and the packet no longer contributes to fluorescence emission. The total number of photon packets detected (usually $10^6$–$10^7$) is defined prior to each simulation.

Medium absorption is included by recalculating the statistical weight of each photon packet that has reached a point of interest within the medium according to its trajectory, i.e.,

$$W(\mathbf{r}) = W_j \exp\left( -\sum_{i=1}^{N_j} \mu_a l_i \right). \tag{3}$$

Here, $N_j$ is the number of scattering events undergone by the $j$'th photon packet during its random walk, $l_i$ is the photon packet path length at the $i$'th scattering event [Eq. (1)], and $W_j$ is the statistical weight of $j$'th photon packet reached at point **r** in the absorption free medium [Eq. (2)]. This approach to separate simulation of scattering and absorption agrees with microscopic Beer–Lambert law, and allows rapid recalculation of the sounding radiation intensity at point **r** for a set of medium absorption.

The MC technique described above was validated through a comparison with the photon diffusion equation for a semi-infinite homogeneous scattering medium.[27] It also demonstrated that when a computational model is used that has reasonable physical and structural parameters typical of skin tissue, the results of skin diffuse reflectance spectra simulation agree reasonably well with the results of *in vivo* skin spectra measurements.[35]

## 3 Simulation of Fluorescence Emission

Typically, computational MC modeling of skin tissue fluorescence consists of three main steps.[16–20] First, the fluence rate distribution within a tissue volume is calculated by the standard MC scheme.[28,29] Then, the spatial fluorescence distribution is obtained by multiplying the fluence rate distribution by

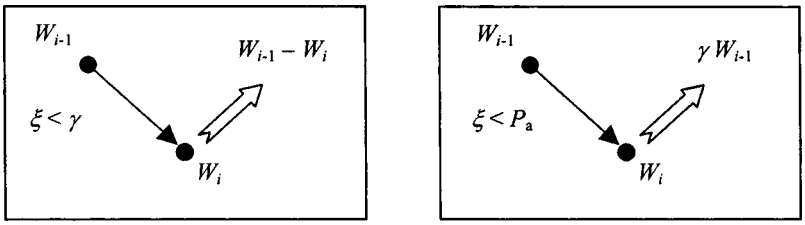



**Fig. 2** Schematic of the fluorescence simulation: (a) fluorescence probability determined by quantum yield $\gamma$ of a fluorophore (Ref. 21); (b) each fluorescence event determined by the probability of the photon packet absorption $P_a=[1-\exp(-\mu_{af}l_i)]$ (Refs. 22 and 23). Here, $W_{i-1}$ and $W_i$ are statistical photon weights at the $(i-1)$'th and $i$'th steps of the photon packet, respectively; $\mu_a^f$ is the fluorophore absorption coefficient; $l_i$ is the path length of a photon between scattering events; $\xi$ $(0\leqslant\xi\leqslant1)$ is the uniformly distributed random number used in the rejection scheme (Ref. 32).

the intrinsic fluorescence profile, which is defined as the product of the absorption coefficient of the fluorophore at the excitation wavelength and its quantum yield at the emission wavelength.[19] Finally, the fluorescence detected is calculated as the convolution of the fluorescence source distribution throughout the tissue with the Green's function.[16–20] With in the framework of this model, the intensity of the simulated local fluorescence is proportional to the fraction of absorbed energy that is determined by the quantum yield of the fluorophore. Thus the fluorescence source distribution within the medium is mainly dependent on the fluence rate distribution.

Crilly et al. employed the MC fluorescence forward-adjoin model.[18] This MC scheme utilizes solution of a transport equation in both the forward (excitation photon) and adjoin (fluorescent photon) calculations. Solution of the adjoin transport equation is obtained for those fluorescence photons that contribute to the fluorescence signal detected.

Recently, another scheme for independent simulation of how fluorescence acts was proposed.[21] In this approach, emission of the fluorescence photons occurs at scattering sites and the quantum yield of a fluorophore $\gamma$ serves as the fluorescence threshold probability [Fig. 2(a)]. The intensity of the simulated fluorescence is defined by the fraction of absorbed radiation $W_{i-1}-W_i$ [see Fig. 2(a)]. In a more plausible model of fluorescence simulation,[22,23] the fluorophore absorption $\mu_a^f$ is separated from total medium/layer absorption by a rejection scheme based on fluorophore absorption threshold $P_a=[1-\exp(-\mu_a^f l_i)]$ [Fig. 2(b)]. Here, the intensity of the fluorescence generated is equal to the product of the quantum yield and the intensity of incident radiation $\gamma W_{i-1}$. In this model, each photon packet produces only one fluorescence photon. Both models assumed that the fluorescence is emitted uniformly from scattering sites in random directions [see Figs. 2(a) and 2(b)].

With regard to the above-mentioned techniques, we extend the MC technique,[27,30] which was briefly described in Sec. 2, for the fluorescence simulation. A schematic of the model is given in Fig. 3. The probability of fluorescence excitation is determined to be

$$W_{\mathrm{em}}(\mathbf{r})=W(\mathbf{r})P_aP_\rho P_\gamma, \tag{4}$$

where $W(\mathbf{r})$, defined by Eq. (3), is the probability that the photon packet has reached point $\mathbf{r}=\mathbf{r}(x,y,z)$ in the medium; $P_a$ is the probability of photon packet absorption at the $i$'th step; $P_\rho$ is the probability of absorption by the fluorophore nonuniformly distributed within the medium; $P_\gamma$ is the probability of fluorescence excitation determined by fluorophore quantum yield $\gamma$. Probabilities $P_a$, $P_\rho$, and $P_\gamma$ are calculated by the standard rejection scheme.[32] In contrast to the above-mentioned models [see Figs. 2(a) and 2(b)], where fluorescence is emitted at the scattering sites, we define the origin of florescence at an arbitrary point $\mathbf{r}(x,y,z)$ between scattering events, i.e., at the absorption site (see Fig. 3). The distribution of fluorophores within human skin is complex.[9,19,26,36] The stratum corneum and the epidermis mainly contain NAD(H), elastin, keratin, flavin, and other fluorophores randomly distributed within these layers.[9,19,36] In dermal layers the spatial distribution of the fluorophore closely follows the distribution of collagen fibers organized in long, wavy bundles, which vary in diameter between 1 and 40 $\mu$m.[37–39] Collagen bundles interweave in a complex random manner and form a three-dimensional irregular meshwork.[37–39] We describe this meshwork by $\cos(k\rho)\cos(kz)$, where $k=\pi/d$; $d$ is the collagen fiber diameter; $\rho=\rho(x,y)$, and $z$ is the coordinate of a point in the medium. The nonhomogeneous distribution of fluorescence within dermal layers is clearly illustrated in the experimental images of autofluorescence of human skin,[19,26] whereas the distribution of fluorophores in the stratum corneum and epidermis seems to be homogeneous.[19] The current MC model neglects all polarization effects that might result in

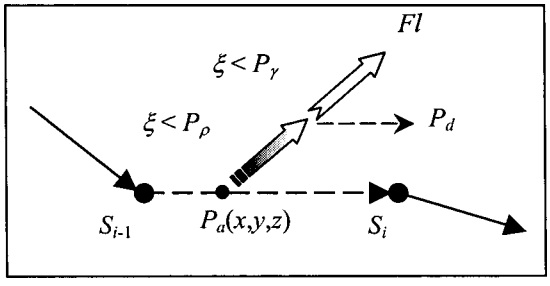



**Fig. 3** Schematic of the fluorescence modeling: $P_a$ is probability of photon packet absorption between two scattering sites $S_{i-1}$ and $S_i$; $P_\rho$ is the probability of absorption by the fluorophore; $P_\gamma$ is the probability of fluorophore fluorescence determined by the fluorophore quantum yield $\gamma$, $P_d=(1-P_\gamma)$ is the probability of dissipation determining a fraction of absorbed energy exerted nonradiative relaxation through other mechanisms, e.g., thermal excitation, etc. or phosphorescence; $\rho(x,y,z)$ determines the spatial fluorophore distribution within the medium.

**Table 1** Optical properties of computational model of skin (Refs. 1–3). ($\mu_s$—scattering coefficient, $\mu_a$—absorption coefficient, $g$—anisotropy factor, $n$—refractive index, $t$—thickness of a layer, $d$—diameter of a collagen fiber, $\gamma$—fluorescence quantum yield.)

| | | $\mu_s$ ($mm^{-1}$) | | | | | | | |
|---|---|---|---|---|---|---|---|---|---|
| $k$ | Skin layer | 488 nm | 700 nm | $\mu_a$ ($mm^{-1}$) | $g$ | $n$ | $t$ ($\mu$m) | $d$ ($\mu$m) | $\gamma$ |
| 1 | Stratum corneum | 40 | 20 | 0.2 | 0.9 | 1.5 | 20 | ⋯ | 0.01 |
| 2 | Epidermis | 35 | 10 | 0.15 | 0.85 | 1.34 | 80 | ⋯ | 0.01 |
| 3 | Sensor layer | 35 | 12 | 0.1 | 0.6 | 1.37 | 50 | ⋯ | 0.5 |
| 4 | Papillary dermis | 30 | 12 | 0.7 | 0.8 | 1.4 | 100 | 3 | 0.15 |
| 5 | Upper blood net dermis | 35 | 15 | 1.0 | 0.9 | 1.39 | 80 | 6 | 0.15 |
| 6 | Dermis | 27 | 12 | 0.7 | 0.76 | 1.4 | 1500 | 20 | 0.15 |
| 7 | Deep blood net dermis | 35 | 15 | 1.0 | 0.95 | 1.39 | 200 | 30 | 0.15 |
| 8 | Subcutaneous fat | 15 | 5 | 0.3 | 0.8 | 1.44 | 5000 | ⋯ | 0.001 |

anisotropic fluorescence emission. Therefore, the fluorescence photons are emitted isotropically from source points, thus agreeing with assumptions proposed in earlier work.[16–24]

When the spatial distribution of fluorescence excitation accumulates as a set of coordinates $(x,y,z)$ and photon weights $W_{\text{em}}$, fluorescence photons are emitted from corresponding fluorescence sources until the necessary number of photon packets collected by a detector is achieved. Emitted fluorescence photons propagate in the medium in a manner similar to that described in Sec. 2.

To express the sensitivity of a surface measurement (a detection system) to the interrogated volume of tissue, detector depth sensitivity, or so-called sampling volume, is employed. The sampling volume $Q(\mathbf{r})$ is defined as the gradient of fluorescent radiation density with respect to the absorption coefficient of a small region of the medium at point (pixel) $\mathbf{r}$.[30,40] It can also be identified with the mean time (or, in other words, the distance) spent by a photon in this region. An intuitive description of detector depth sensitivity can be obtained in terms of the accumulated trajectories of fluorescence photons that reach the detector that make it amenable to calculation using the Monte Carlo method as follows:

$$Q(\mathbf{r}) = -\frac{\partial}{\partial \mu_a(\mathbf{r})} \ln\left(\frac{I}{I_0}\right) = \frac{\Sigma_{j=1}^{M} l_j(\mathbf{r}) W_j'}{l_0 \Sigma_{j=1}^{M} W_j'}. \qquad (5)$$

Here $W_j'$ is the final weight of the $j$'th fluorescence photon packet calculated by Eqs. (2) and (3) with the initial weight determined by $W_{\text{em}}$ [Eq. (4)]; $M$ is the total number of detected fluorescence photon packets; $l_j(\mathbf{r})$ is the weighted mean of path length traversed by a photon packet in a cell with its center position at $\mathbf{r}$; $l_0$ is the size of the cell, which has cubic shape of 10 $\mu$m×10 $\mu$m×10 $\mu$m. In the results of simulation presented below, the sampling volume $Q(\mathbf{r})$ is considered a two-dimensional cross-sectional map $Q(x,z)$ because of its three-dimensional (3-D) distribution, where $x$ is the horizontal axis and $z$ is the depth direction.

## 4 Results and Discussion

The MC model described was used to assess the spatial distribution of both skin tissue autofluorescence and fluorescence excitation of the tattoo sensor layer. The optical parameters of skin tissue used in the simulation are shown in Table 1. These parameters were chosen for 488 nm, whereas optical properties of the sensor layer were assumed to be close to the optical characteristics of the most dominant fluorophores used in clinical diagnostics.[9,41] The 488 nm wavelength was used as the excitation wavelength, since it is close to the fluorescein absorption maximum (494 nm). The tattoo sensor layer, embedded in the epidermis (100–150 $\mu$m), is 50 $\mu$m thick and the thickness of the pure epidermis is 80 $\mu$m (see Table 1 for details). Actually, the optical tissue properties for excitation and emission (fluorescence) wavelengths are different. In the visible/near-infrared range of the spectrum scattering coefficient $\mu_s$ is a slowly varying function of the wavelength.[42,43] In this study these parameters are assumed to be identical, since they are intended to illustrate general trends of changes in the detecting signal localization due to refractive index matching rather than provide a detailed quantitative analysis. This assumption is justified if the Stokes' shift is less than 100 nm.[44]

The simulated distribution of fluorescence excitation obtained within the skin has a distinct porous periodical structure in the dermal layers (Fig. 4). This is the consequence of the collagen meshwork modeled as a periodic function. The period of this structure is close to the collagen bundle diameter of modeled layers, 20 $\mu$m (see Table 1). The distribution of the fluorescence excitation in the papillary dermis seems highly granular, and the fine porous structure is only marginally observed. The papillary dermis lies at 150–250 $\mu$m depth and contains small (0.3–3 $\mu$m in diameter) loosely distributed collagen fibers.[37–39] Modeled autofluorescence excitation observed in the dermal layers is significantly higher than in stratum corneum and epidermis. This agrees well with experimental data.[19,25,26] However, the excitation of fluorescence in

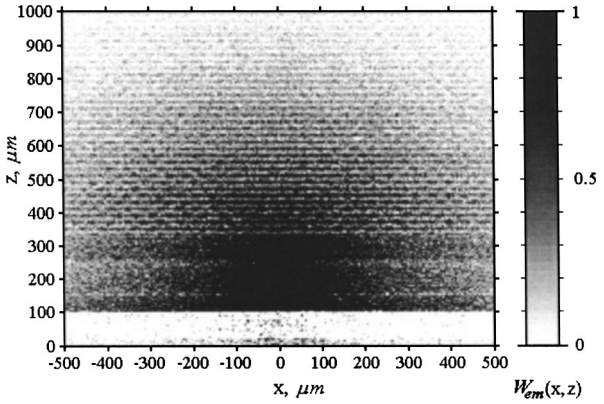



**Fig. 4** Spatial distribution $W_{em}(x,z)$ of the fluorescence excitation of the tattoo sensor layer embedded in the epidermis and autofluorescence excitation in human skin. Optical parameters of the model were chosen for 488 nm (see Table 1). The diameters of collagen bundles were chosen as 3, 6, 20, and 30 $\mu$m in papillary dermis, upper blood net dermis, dermis, and deep blood net dermis, respectively. The diameter of the source is equal to 200 $\mu$m. The incident beam has a uniform geometry profile.

sensor (100–150 $\mu$m) and in dermal layers (250–330 $\mu$m) is comparable quantitatively (see Fig. 4).

Regardless of the complex porous periodical structure of the fluorescence excitation distribution (see Fig. 4), the corresponding sampling volume seems to be smooth and continuous (Fig. 5). As expected, the area of maximum sensitivity is localized in the sensor and topical dermal layers (up to ~300 $\mu$m under the surface, i.e., papillary and upper blood net derma). However, the fraction of fluorescence that is sensitive to sensor and topical dermal layers is almost identical (see Fig. 5). Accordingly, for adequate quantitative interpretation of the fluorescence signal detected differential analysis is required.

Additional MC simulation was carried out to illustrate how the localization of fluorescence excitation and sampling volume are affected by excitation at longer wavelength. To do

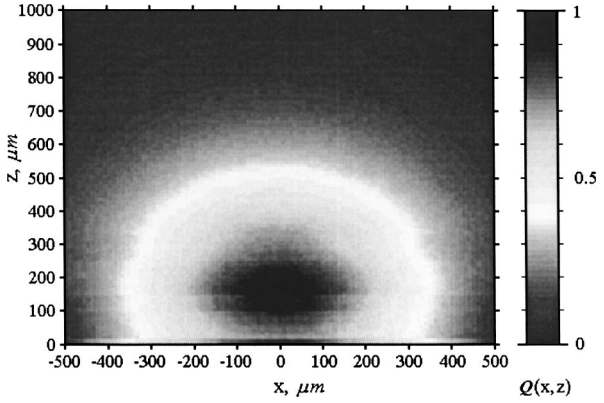



**Fig. 5** Two-dimensional distributions of the spatial depth sensitivity $Q(x,z)$. The optical parameters of skin layers were chosen for 488 nm (Table 1). The fraction of fluorescence that is sensitive to sensor and topical dermal layers is close to one another. The diameter and numerical aperture of the detector are equal to 1000 $\mu$m and 0.63; acceptance angle $\theta_d = \sin^{-1}(\mathrm{NA}/n_0)$ is 40° with NA the numerical aperture.

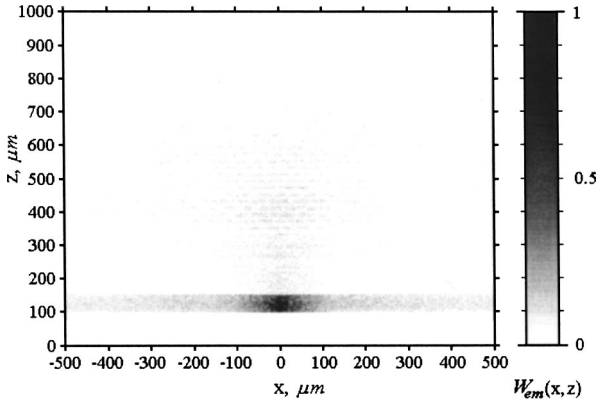



**Fig. 6** Spatial distribution $W_{em}(x,z)$ of the fluorescence excitation of the tattoo sensor layer and autofluorescence excitation in human skin in the near-infrared spectral region. Excitation of the autofluorescence in the dermal layers is highly (~four to five times) suppressed due to the low fluorescence efficiency of natural fluorophores in the near-infrared spectral region (Ref. 9). The main fluorescence excitation is localized in the sensor layer. The modeled optical skin tissue properties were chosen for 700 nm (see Table 1). Absorption coefficients $\mu_a$ skin layers are taken to be a factor of 10 less (Ref. 1). Scattering coefficients $\mu_s$ are reduced by a factor of 2–3. The rest of the optical skin tissue parameters are held constant. Scattering of the sensor layer is chosen to be equal to that of the epidermis. Its absorption coefficient is held constant assuming use of a near-infrared fluorophore. The diameter of the source is equal to 200 $\mu$m. The incident beam has a uniform geometry profile.

this modeled optical skin tissue properties were chosen for 700 nm. Due to the monotonic decrease in scattering of skin tissue with the wavelength in the range of 450–1100 nm,[42,43] scattering coefficients $\mu_s$ are reduced by a factor of 2–3, whereas the absorption coefficients of the skin layers are taken to be a factor of 10 less[1] (see Table 1 for details). The rest of the optical parameters of skin tissue were held constant. Scattering of the sensor layer was believed to be similar to that of the epidermis, while its absorption coefficient was assumed to be unchanged, presuming use of a near-infrared fluorophore.[45] The low fluorescence efficiency of endogenous fluorophores in the near-infrared spectral region[9] was simulated by their reduced absorption; the quantum yield of biotissues was kept unchanged thoughout.

The results of the simulation are presented in Fig. 6. The results show that the excitation of autofluorescence in the dermal layers is highly (~four to five times) suppressed due to the low fluorescence efficiency of natural fluorophores in the near-infrared spectral region[9] and that the main fluorescence excitation is localized in the sensor layer. Nevertheless, the complex porous periodic structure in the dermal layers is still observed. Results of the sampling volume analysis demonstrate that the maximum for detecting the depth sensitivity is localized in a small region deep in the sensor layer (Fig. 7). In other words, the detector predominantly collects those fluorescence photons that are generated in the sensor layer. However, the presence of a contribution from stratum corneum and epidermis is also non-negligible (see Fig. 7).

Recently it has been demonstrated that localization of the signal detected can significantly be improved by so-called skin tissue clearing.[46,47] Diffusion of biocompatible chemicals into skin temporarily substitutes for water within tissues. This

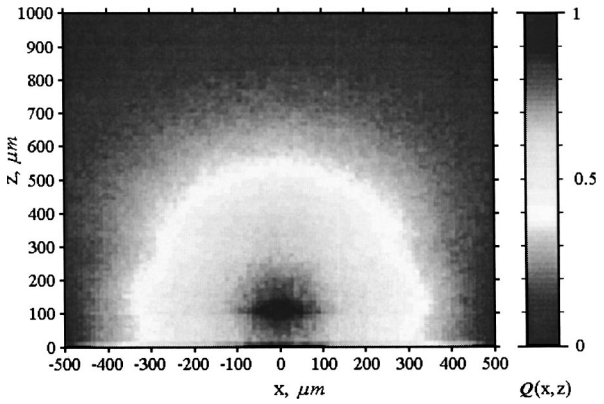



**Fig. 7** Two-dimensional distributions of the spatial depth sensitivity $Q(x,z)$ in the near-infrared spectral region. The maximum detecting depth sensitivity is localized in a small region deep in the sensor layer. The detector predominantly collects those fluorescence photons that are generated in the sensor layer. The optical parameters of skin layers were chosen for 700 nm (Table 1). The diameter and numerical aperture of the detector are equal to 1000 $\mu$m and 0.63; acceptance angle $\theta_d = \sin^{-1}(\mathrm{NA}/n_0)$ is 40°.

causes matching of the refractive indices of the structural elements of skin cells (not the medium surface as in our case) and temporarily increases the transparency of upper skin layers that allows unrestricted light to permeate deeper into tissues.[46,47] A considerable increase of detected fluorescence signal was observed since the scattering in skin tissue was substantially reduced through the application of biochemical clearing agents.[48] By the way, the results presented in Fig. 7 can be also considered from this point of view, i.e., how the reducing of scattering affects the sampling volume.

Contrary to the tissue clearing approach, lately, researchers' attention has been drawn to matching refractive indices at the medium boundary interface.[27,49,50] In the current study the effect of matching of the refractive index is also examined by using additional modeling. The simulation is repeated using identical optical parameters of skin layers chosen for 488 and 700 nm. The refractive index of an adjacent medium was taken as equal to the refractive index of the stratum corneum, i.e., 1.5. The outcomes of simulation (Fig. 8) show that the refractive index matching does not change the distributions of fluorescence excitation much compared to those depicted in Figs. 4 and 6. They are explained by the fact that there is a low fluorophore concentration in the topical skin layers, and these layers have mostly undergone refractive index matching.[27]

The results of the sampling volume simulation for the case of refractive indices matching are presented in Fig. 9. Matching of the refractive indices of the ambient medium and stratum corneum restricts localization of detector depth sensitivity in the sensor layer and upper dermal layer, and removes it from stratum corneum and epidermis [see Fig. 5 vs Figs. 9(a) and Fig. 7 vs Fig. 9(b)]. It can be seen that the sampling volumes have remained constant, but the maximum of detector depth sensitivity was shifted to the sensor layer. That should result in detection of the fluorescence signal emitted from the tattoo sensor.

## 5 Conclusions

We have studied the localization of fluorescence probing in a small predictable volume for express noninvasive skin tissues monitoring. The MC technique was applied to model the fluorescence excitation and to assess the sampling volume within the skin. The results of simulation show that maximum of the fluorescence excitation sources is localized in topical dermal layers and in the tattoo sensor. The spatial distribution of the fluorescence excitation within dermal layers demonstrated a

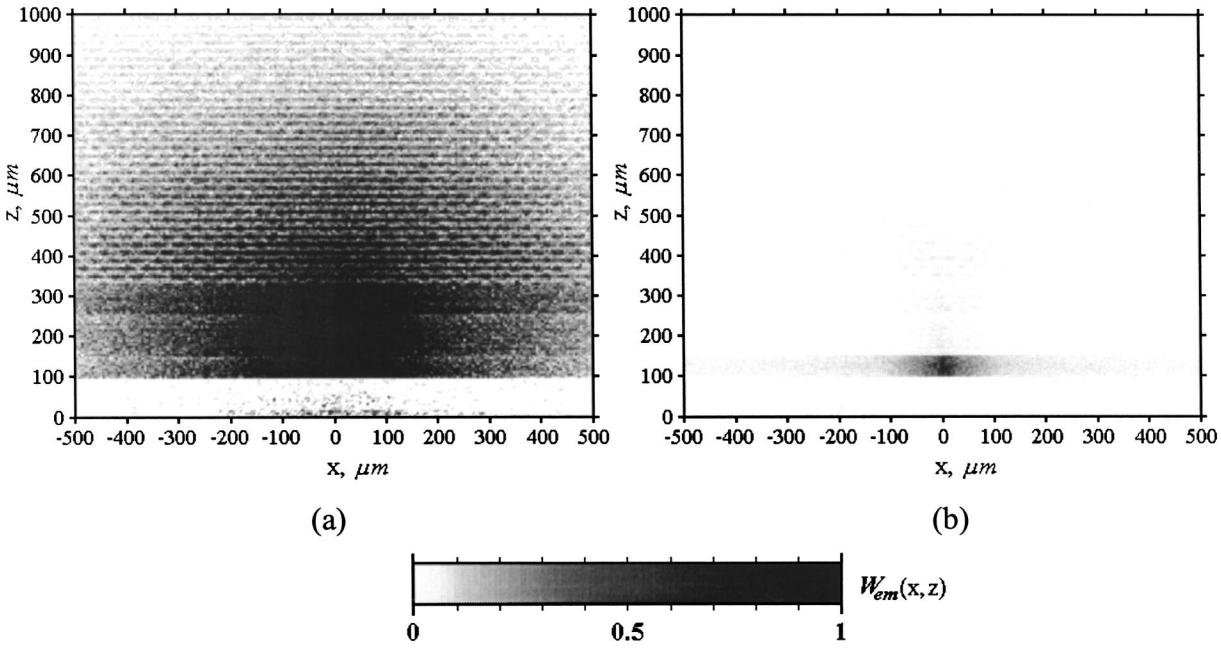



**Fig. 8** Spatial distribution of the fluorescence excitation for refractive index matching ($n_0 = 1.5$): (a) visible spectral region 488 nm; (b) near-infrared spectral region 700 nm.

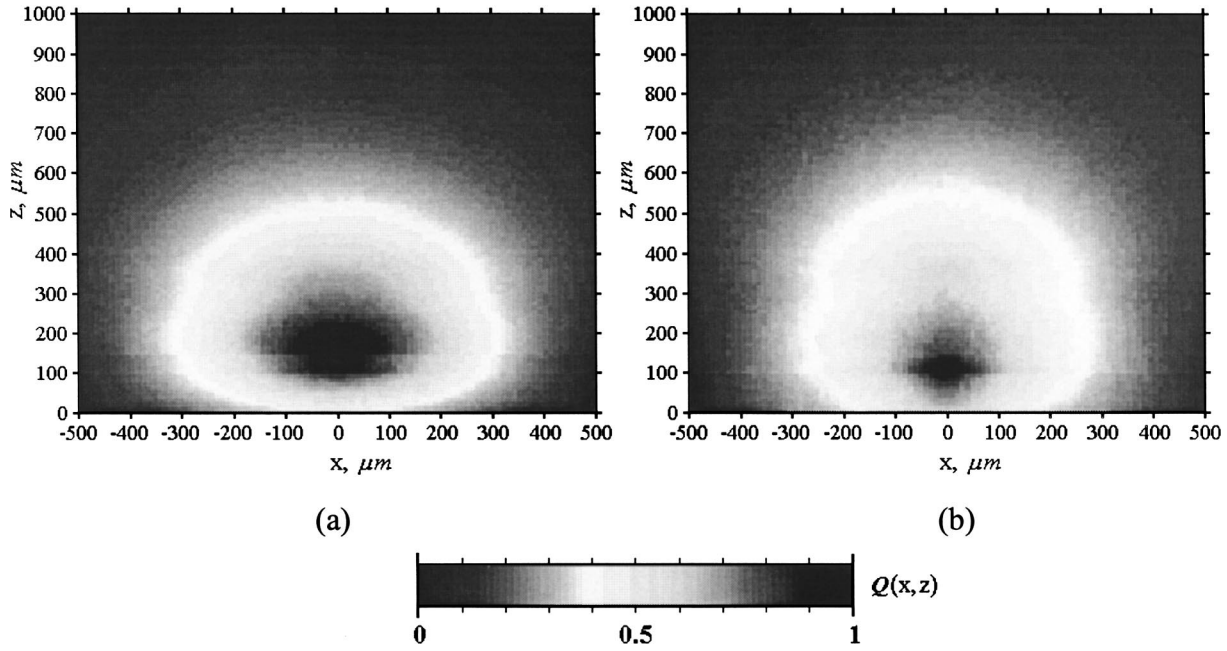



**Fig. 9** Two-dimensional distributions of the spatial depth sensitivity $Q(x,z)$ for refractive index matching ($n_0=1.5$): (a) visible spectral region 488 nm; (b) near-infrared spectral region 700 nm. Matching of the refractive indices of the ambient medium to the stratum corneum restricts localization of the detector depth sensitivity in the sensor layer and upper dermal layer, and removes it from the stratum corneum and epidermis (see Figs. 5 and 7). The regions sampled by fluorescence radiation have remained constant; the maximum of detector depth sensitivity is shifted to the sensor layer. It leads to the detection of more fluorescence photons emitted from the tattoo sensor layer. The diameter and numerical aperture of the detector are equal to 1000 $\mu$m and 0.63; acceptance angle $\theta_d=\sin^{-1}(\mathrm{NA}/n_0)$ is 25°.

good correlation to an experimental autofluorescence image of skin tissue.[19] By moving to a near-infrared spectral region, the fraction of autofluorescence excitation is significantly reduced and a sampled area is localized predomintly in the tattoo sensor layer. The effect of refractive index matching at the skin interface produces a remarkable enhancement of sampling volume localization. The maximum of detector depth sensitivity is shifted to the tattoo sensor layer, and is removed from the stratum corneum and epidermis.

Simulations have revealed a general tendency of optical/fluorescence measurements to localize in a small shallow volume in the tattoo sensor layer. We believe that the results of this study accompanied by recent progress in skin optics[46–48] could be beneficial to a number of applications for medical diagnostic and general physiological studies.

## References


1. V. Tuchin, *Tissue Optics: Light Scattering Methods and Instruments for Medical Diagnosis*, Vol. TT38, SPIE Bellingham, WA (2000).
2. W. F. Cheong, S. A. Prahl, and A. J. Welch, ''A review of the optical properties of biological tissues,'' *IEEE J. Quantum Electron.* **26**(12), 2166–2185 (1990).
3. M. J. C. van Gemert, S. L. Jacques, H. J. C. M. Sterenborg, and W. M. Star, ''Skin optics,'' *IEEE Trans. Biomed. Eng.* **36**(12), 1146–1154 (1989).
4. S. L. Jacques, ''Origins of tissue optical properties in the UVA, visible, and NIR regions,'' in *OSA Topics on Advances in Optical Imaging and Photon Migration*, R. R. Alfano and J. G. Fujimoto, Eds., Vol. 2, pp. 364–369, OSA (1996).
5. R. R. Anderson and L. S. Parrish, ''Optical properties of human skin,'' in *The Science of Photomedicine*, J. D. Regan and J. A. Parrish, Eds., pp. 147–194, Plenum, New York (1982).
6. R. W. Waynant, *Lasers in Medicine*, Chemical Rubber, Boca Raton, FL (2002).
7. Y. Mendelson, ''Biomedical sensors,'' in *Introduction to Biomedical Engineering*, J. D. Enderle, S. M. Blanchard, and J. D. Bronzino, Eds., Chap. 4, pp. 139–178, Academic, New York (2000).
8. I. V. Meglinski, S. A. Piletsky, D. A. Greenhalgh, and A. P. F. Turner, ''Vanishing 'tattoo' sensors for medical diagnostics,'' *Proc. Second International Workshop on Molecularly Imprinted Polymers*, p. 55, La Grande Motte, France (2002).
9. J. R. Lakowicz, *Principles of Fluorescence Spectroscopy*, Plenum, New York (1999).
10. O. Panou-Diamandi, N. K. Uzunoglu, G. Zacharakis, G. Filippidis, T. Papazoglou, and D. Koutsouris, ''One-layer tissue fluorescence model based on the electromagnetic theory,'' *J. Electromagn. Waves Appl.* **12**(8), 1101–1121 (1998).
11. A. J. Durkin, S. Jaikumar, N. Ramanujam, and R. Richards-Kortum, ''Relation between fluorescence-spectra of dilute and turbid samples,'' *Appl. Opt.* **33**(3), 414–423 (1994).
12. J. Wu, M. S. Feld, and R. P. Rava, ''Analytical model for extracting intrinsic fluorescence in turbid medium,'' *Appl. Opt.* **32**(19), 3585–3595 (1993).
13. D. E. Hyde, T. J. Farrell, M. S. Patterson, and B. C. Wilson, ''A diffusion theory model of spatially resolved fluorescence from depth-dependent fluorophore concentrations,'' *Phys. Med. Biol.* **46**(2), 369–383 (2001).
14. M. S. Nair, N. Ghosh, N. S. Raju, and A. Pradhan, ''Determination of optical parameters of human breast tissue from spatially resolved fluorescence: A diffusion theory model,'' *Appl. Opt.* **41**(19), 4024–4035 (2002).
15. A. H. Gandjbakhche, R. F. Bonner, R. Nossal, and G. H. Weiss, ''Effects of multiple-passage probabilities on fluorescent signal from biological media,'' *Appl. Opt.* **36**(19), 4613–4619 (1997).
16. R. Richards-Kortum, ''Fluorescence spectroscopy of turbid media,'' in *Optical–Thermal Response of Laser Irradiate Tissue*, A. J. Welch and M. J. C. van Gemert, Eds., pp. 667–707, Plenum, New York (1995).
17. J. Qu, C. MacAulay, S. Lam, and B. Palcic, ''Laser-induced fluorescence spectroscopy at endoscopy: Tissue optics, Monte Carlo modelling, and *in vivo* measurements,'' *Opt. Eng.* **34**(11), 3334–3343 (1995).
18. R. J. Crilly, W. F. Cheong, B. Wilson, and J. R. Spears, ''Forward-

adjoin fluorescence model: Monte Carlo integration and experimental validation,'' *Appl. Opt.* **36**(25), 6513–6519 (1997).
19. H. Zeng, C. MacAulay, D. I. McLean, and B. Palcic, ''Reconstruction of *in vivo* skin autofluorescence spectrum from microscopic properties by Monte Carlo simulation,'' *J. Photochem. Photobiol., B* **38**(3), 234–240 (1997).
20. A. J. Welch, C. Gardner, R. Richards-Kortum, E. Chan, G. Criswell, J. Pfefer, and S. Warren, ''Propagation of fluorescent light,'' *Lasers Surg. Med.* **21**(2), 166–178 (1997).
21. M. J. McShane, S. Rastegar, M. Pishko, and G. L. Cote, ''Monte Carlo modeling of implantable fluorescent analyte sensors,'' *IEEE Trans. Biomed. Eng.* **47**(5), 624–632 (2000).
22. B. Pogue and G. Burke, ''Fiber-optic bundle design for quantitative fluorescence measurement from tissue,'' *Appl. Opt.* **37**(31), 7428–7436 (1998).
23. K. Vishwanath, B. Pogue, and M. A. Mycek, ''Quantitative fluorescence spectroscopy in turbid media: Comparison of theoretical, experimental and computational methods,'' *Phys. Med. Biol.* **47**(18), 3387–3405 (2002).
24. Y. P. Sinichkin, S. R. Utz, I. V. Meglinskii, and E. A. Pilipenko, ''Spectroscopy of human skin *in vivo*. II. Fluorescence spectra,'' *Opt. Spectrosc.* **80**(3), 383–389 (1996).
25. Y. P. Sinichkin, N. Kollias, G. I. Zonios, S. R. Utz, and V. V. Tuchin, ''Reflectance and fluorescence spectroscopy of human skin *in vivo*,'' in *Handbook of Optical Biomedical Diagnostics*, V. V. Tuchin, Ed., Vol. PM107, pp. 727–785, SPIE, Bellingham, WA (2002).
26. H. Zeng, C. MacAulay, D. I. McLean, and B. Palcic, ''Spectroscopic and microscopic characteristics of human skin autofluorescence emission,'' *Photochem. Photobiol.* **61**(6), 639–645 (1995).
27. D. Y. Churmakov, I. V. Meglinski, and D. A. Greenhalgh, ''Influence of refractive index matching on the photon diffuse reflectance,'' *Phys. Med. Biol.* **47**(23), 4271–4285 (2002).
28. R. Graaf, M. H. Koelink, F. F. M. de Mul, W. G. Zijlstra, A. C. M. Dassel, and J. G. Aarnoudse, ''Condensed Monte Carlo simulations for the description of light transport,'' *Appl. Opt.* **32**(4), 426–434 (1993).
29. L. Wang, S. L. Jacques, and L. Zheng, ''MCML—Monte Carlo modelling of light transport in multi-layered tissues,'' *Comput. Methods Programs Biomed.* **47**(2), 131–146 (1995).
30. I. V. Meglinsky and S. J. Matcher, ''Modelling the sampling volume for skin blood oxygenation measurements,'' *Med. Biol. Eng. Comput.* **39**(1), 44–50 (2001).
31. I. V. Meglinskii and S. J. Matcher, ''Analysis of the spatial distribution of the detector sensitivity in a miltilayer randomly inhomogeneous medium with strong light scattering and absorption by the Monte Carlo method,'' *Opt. Spectrosc.* **91**(4), 654–659 (2001).
32. I. M. Sobol', *The Monte Carlo Method*, The University of Chicago Press, Chicago (1974).
33. L. G. Henyey and J. L. Greenstein, ''Diffuse radiation in the galaxy,'' *Astrophys. J.* **93**, 70–83 (1941).
34. M. Born and E. Wolf, *Principles of Optics*, Cambridge University Press, Cambridge (1999).
35. I. V. Meglinski and S. J. Matcher, ''Quantitative assessment of skin layers absorption and skin reflectance spectra simulation in visible and near-infrared spectral region,'' *Physiol. Meas* **23**(4), 741–753 (2002).
36. A. R. Young, ''Chromophores in human skin,'' *Phys. Med. Biol.* **42**(5), 789–802 (1997).
37. L. T. Smith, K. A. Holbrook, and P. H. Byers, ''Structure of dermal matrix during development and in the adult,'' *J. Invest. Dermatol.* **79**, 930–1040 (1982).
38. G. F. Odland, ''Structure of the skin,'' in *Physiology, Biochemistry, and Molecular Biology of the Skin*, L. A. Goldsmith, Ed., Vol. 1, pp. 3–62, Oxford University Press, Oxford (1991).
39. W. Montagna, A. M. Kligman, and K. S. Carlisle, *Atlas of Normal Human Skin*, Springer, Berlin (1992).
40. S. R. Arridge, ''Photon-measurement density functions. Part I: Analytical forms,'' *Appl. Opt.* **34**(31), 7395–7409 (1995).
41. H. Schneckenburger, K. Stock, R. Steiner, W. Strauss, and R. Sailer, ''Fluorescence technologies in biomedical diagnostics,'' in *Handbook of Optical Biomedical Diagnostics*, V. V. Tuchin, Ed., Vol. PM107, pp. 825–874, SPIE, Bellingham, WA (2002).
42. C. R. Simpson, M. Kohl, M. Essenpreis, and M. Cope, ''Near-infrared optical properties of *ex vivo* human skin and subcutaneous tissues measured using the Monte Carlo inversion technique,'' *Phys. Med. Biol.* **43**(9), 2465–2478 (1998).
43. R. M. P. Doornbos, R. Lang, M. C. Aalders, F. M. Cross, and H. J. C. M. Sterenborg, ''The determination of *in vivo* human tissue optical properties and absolute chromophore concentrations using spatially resolved steady-state diffuse reflectance spectroscopy,'' *Phys. Med. Biol.* **44**(4), 967–981 (1999).
44. M. S. Patterson and B. W. Pogue, ''Mathematical model for time-resolved and frequency-domain fluorescence spectroscopy in biological tissues,'' *Appl. Opt.* **33**(10), 1963–1974 (1994).
45. G. A. Casay, D. B. Shealy, and G. Patonay, ''Near-infrared fluorescence probes,'' in *Topics in Fluorescence Spectroscopy*, J. R. Lakowicz, Ed., Vol. 4, pp. 183–222, Plenum, New York (1994).
46. I. V. Meglinski, A. N. Bashkatov, E. A. Genina, D. Y. Churmakov, and V. V. Tuchin, ''The enhancement of confocal images of tissues at bulk optical immersion,'' *Laser Phys.* **13**(1), 65–69 (2003).
47. R. K. Wang, X. Xu, V. V. Tuchin, and J. B. Elder, ''Concurrent enhancement of imaging depth and contrast for optical coherence tomography by hyperosmotic agents,'' *J. Opt. Soc. Am. B* **18**(7), 948–953 (2001).
48. G. Vargas, K. F. Chan, S. L. Tomsen, and A. J. Welch, ''Use of osmotically active agents to alter optical properties of tissue: Effects on the detected fluorescence signal measured through skin,'' *Lasers Surg. Med.* **29**(3), 213–220 (2001).
49. T. J. Farrell and M. S. Patterson, ''Experimental verification of the effect of refractive index mismatch on the light fluence in a turbid medium,'' *J. Biomed. Opt.* **6**(4), 468–473 (2001).
50. A. Godavarty, D. J. Hawrysz, R. Roy, E. M. Sevick-Muraca, and M. J. Eppstein, ''Influence of the refractive index mismatch at the boundaries measured in fluorescence enhanced frequency-domain photon migration imaging,'' *Opt. Express* **10**(15), 653–661 (2002).



https://dspace.org/

# Amending of fluorescence sensor signal localization in human skin by matching of the reflective index.

**Churmakov, D. Y.; Meglinski, Igor V.; Greenhalgh, Douglas A.**

**2004-01-01T00:00:00Z**
Society of Photo-Optical Instrumentation Engineers (SPIE)
https://doi.org/10.1117/1.1645796
Churmakov D Y, Meglinski I V and Greenhalgh D A (2004) Amending of fluorescence sensor signal localization in human skin by matching of the refractive index, Journal of Biomedical Optics, 9 (2): 339-346,

Downloaded from a DSpace repository. https://dspace.org/